Dielectric relaxation behaviour and ionic conductivity for corn starch and PVP with sodium fluoride

M. Nandhinilakshmi[1], D. Vanitha[2,*] , N. Nallamuthu[2], K. Sundaramahalingam[3], and P. Saranya[1]

[1] *Multi-Functional Materials Laboratory, International Research Centre, Kalasalingam Academy of Research and Education, Krishnankoil, Tamilnadu 626 126, India*

[2] *Department of Physics, Kalasalingam Academy of Research and Education, Krishnankoil, Tamilnadu 626 126, India*

[3] *Department of Physics, Arulmigu Kalasalingam College of Arts and Science, Krishnankoil, Tamilnadu 626 126, India*

ABSTRACT

Biopolymer electrolytes based on cornstarch and polyvinyl pyrrolidone blend with different weight per cent of sodium fluoride salt were synthesized using solution casting technique. The amorphous nature of the polymer blend with the addition of NaF had been studied by X-ray diffraction studies. Fourier Transform Infrared studies helped to discover the presence of functional groups and the complex formation between the bonding of polymers chains. Using AC impedance analyzer, the dielectric behaviour was recorded in the frequency (1 Hz–1 MHz) and various ranges of temperature (303–373 K). The ionic conductivity was improved with the increase of salt concentration as well as temperature. The maximum conductivity of 4.6629×10^{-4} S cm^{-1} was obtained for 15 wt% of sodium fluoride-added electrolyte. The temperature dependence of conductivity for polymer electrolyte films has followed the Arrhenius relation and minimum activation energy of 0.1775 eV was noted for the sodium fluoride-added sample. Relaxation time (τ) was identified from the tangent loss peak observed at 303 K. Wagner's DC polarization technique confirmed that the conductivity was due to the ions. The modulus spectra indicated the Non-Debye nature of the electrolytes. Argond plot investigated the relaxation process. Electrochemical stability was confirmed by Cyclic voltammetry.

1 Introduction

Recent research is based on solid electrolytes for numerous applications like a weightless battery with high voltage, and also focussed on whether it has biodegradable properties which help to reduce land pollution. For this reason, we prefer biopolymer electrolytes based on extracts such as starch and green gum. Normally, every biological substance (polymer) has ionic-conductive properties that are essential for ionic motion [1].

Address correspondence to E-mail: vanibala2003@gmail.com

The structure of the battery comprises two electrodes separated by an electrolyte. Our work focuses on biopolymer electrolytes for energy storage devices [2]. The best characteristic of solid polymer electrolytes is that it does not react with electrodes. Several applications for energy storage devices are fuel cells, solar cells, portable batteries, sensors, power banks, and supercapacitors [3].

Synthetic polymers such as PEO, PVdF, PVA, and PAN are often used as a polymer host in solid polymer electrolytes, which are non-biodegradable and toxic and can cause environmental problems. The remedy for environmental pollution is to use natural polymers such as chitosan, starch, pectin, agar, methylcellulose, and cellulose acetate, which have been suggested by researchers to form Solid Biopolymer electrolytes [4–8].

Corn starch is a natural polymer starch. It is used as the host polymer for electrolytes. Starch is usually formed in plants by photosynthesis. Corn flour contains amylose (poly-α-1, 4-d-glucopyranoside) and the bronchodilator and amylopectin (poly-α-1, 4-d glucopyranoside and α-1, 6-di-glucopyranoside) Corn starch (CS) is a semi-crystalline polymer that consists of two chains, a linear amylase, and a chain of branched amylopectin [9–11].

Polyvinylpyrrolidone (PVP) is used as a blend polymer to improve the deformation for ionic mobility. Polyvinylpyrrolidone (PVP) is a polymer that combines exceptional possibilities such as eco-friendliness, easy processing, and complex-forming capabilities [3, 12–14]. The side chains of PVP contain a carbonyl group (C=O), which helps to create different complexes with different mineral salts. It interacts more with different types of ions and increases the number of free ions in the system [15, 16].

The Sodium fluoride (NaF) is added to the blend polymer electrolyte to further increase the conductivity value. Sodium-bonded biopolymer electrolytes are a probable competitor to replace lithium ion-based batteries owing to the low cost of sodium in battery application [6, 17]. NaF with a synthetic polymer such as PVA–PVP has been reported by the incorporation of salt with blend polymer [18]. PVP–PVA with 2 wt% of NaF blend electrolyte reported the conductivity of 10^{-4} S cm^{-1} [19] and PVP–PEO blend and NaF shows maximum conductivity of 10^{-8} S cm^{-1} [20]. From the earlier reports, it is confirmed that the blend of 80 wt% cornstarch and 20 wt% PVP

is having the high conductivity of 4.90217×10^{-9} S cm^{-1} and low activation energy (0.16 eV) [21]. For the environmental friendly purpose and to increase maximum conductivity of electrolytes, 80 wt% Cornstarch:20 wt% PVP blend polymer electrolytes has prepared as blend polymer and then salt is added to the system to attain the maximum conductivity in the range of 10^{-4} S cm^{-1} [11].

2 Experimental method

2.1 Materials

Cornstarch with monomer $C_6H_{10}O_5$ was purchased from SRL chemicals (SISCO RESEARCH LABORATORIES PVT. LTD) with NF grade and PVP with monomer C_6H_9NO was procured from Sd fine-chem. Ltd., India (SDFCL) with USP grade. 98.5% purity of Sodium fluoride was procured from oxford laboratory chem. Ltd and double-distilled water is used as a solvent.

2.1.1 Characterization technique

X-Ray diffractometer designed by Bruker was used to confirm the phase structure of the polymer electrolyte. This instrument scanned in the range of 2 = 10° to 60° at a rate of 5° per minute with CuKa radiation. To evaluate the complication, The SHIMADZU IR Tracer 100 spectrometer was used to observe FTIR spectra with a resolution of 4 cm^{-1} at wavenumbers ranging from 4000 to 400 cm^{-1}. The ionic conductivity and dielectric properties of the polymer electrolytes were investigated using a computer-controlled HIOKI 3532 LCR metre in the temperature range of 303–368 K and a frequency range of 42 Hz–1 MHz. Using the CH-Instrument Model 6008e, the electrochemical property of the sample was examined using cyclic voltammetry (CV).

2.2 Preparation method

The solution casting technique was used for the preparation of solid biopolymer electrolyte (SBE). Using magnetic stirrer, 80 wt% of cornstarch was dissolved by 30 ml of deionized water with 0.42 ml acetic acid for 20 min at 85 °C. At the same time 20 wt% of PVP was dissolved in 20 ml of deionized water for 1 h at room temperature and different X (5,

10, 15, and 20) wt% of sodium fluoride (NaF) was dissolved in 10 ml of deionized water. The solutions were mixed by a 1-h time interval to make a homogenous solution. The final dissolution was poured into a 50 mm Petri dish and placed without any disturbance for 8 days to evaporate the solvent. The prepared electrolytes were kept in desiccators for further characterization. The image of the prepared solid polymer electrolyte is given in Fig. 1a. The possible chemical interaction with the blend polymer chain and sodium fluoride salt is given in Fig. 1b. The details of the quantity of chemicals in gms for the preparation of PBE are given in Table 1 rather the wt%.

3 Result and discussion

3.1 XRD

XRD helps to study the impact of various wt% of sodium fluoride salt with 80 wt% CS:20 wt% PVP (CS/PVP) blend polymer sample which is observed in the diffraction pattern in the angle of 10°–60° range. The recorded patterns are shown in Fig. 2. The sample code CPF5, CPF10, CPF15, and CPF20 stands for the prepared solid polymer electrolyte with 5, 10, 15, and 20 wt% of NaF salt, respectively. The observed XRD pattern confirms the presence of Cornstarch which are having humps at 16.8°, 19.5°, 21.8° [22], and the appeared broad hump at 30.5° for PVP [23]. The intensity of the humps is decreased by increasing the salt concentration. For CPF 15, the intensity of humps related to CS is decreased and the hump related to PVP is slightly increased. The amorphous nature of the blend polymer is increased while increasing the wt% of sodium fluoride salt up to the CPF15 sample. After increasing the salt concentration, the CPF20 electrolyte shows the new peak at 31° and 39° which is due to the NaF salt which is confirmed using JCPDS no-36-1455 [14, 23, 24]. The absence of peaks representing NaF up to CPF15 ensures the thorough dissipation of NaF salt in the blend polymer system [24, 25]. As the NaF salt concentration is increased for CPF20 Sample, a peak at 31° tends to appear resulting in a decrease in ionic conductivity.

3.2 FT-infrared analysis

The functional groups and structure identification can be carried out based on FTIR spectral analysis. Figure 3a depicts the vibrational bands present in CS/PVP blend with different sodium fluoride concentrations. Observed FTIR transmission bands of all-polymer electrolytes are explained in Table 2. The wide bands of the hydroxyl group (O–H) stretching for the sample are reported at 3323 cm^{-1} [26]. The vibrational band are recognized at 2924 cm^{-1}, 1655 cm^{-1}, 1427 cm^{-1}, and 1422 cm^{-1} which corresponds to CH$_2$ asymmetric stretching, C=O, C–H, and CH$_2$ wagging stretching, respectively [27, 28].

Figure 3b clearly shows the vibrational bands in the 1800–600 cm^{-1} range. The band corresponding to C–N stretching is observed at 1288 cm^{-1}. The intensity of the C–C stretching get increased and this band is located at 1001 cm^{-1} and C–O in C–O–C stretching observed at 995 cm^{-1} for all the prepared samples.

The C–O stretching for the salt-added sample is observed at 1151 cm^{-1}. The vibration band observed at 1560 cm^{-1} is assigned to C=C Stretching and the band at 646 cm^{-1} is assigned to CF$_2$ bending [29]. This band represents the evidence of the complexation and interaction of the polymer blend system with NaF salt on the chemical structure of the electrolyte.

3.2.1 FT-infrared deconvolution

Origin 8.5 fitting software is used to execute the deconvolution method, which is based on the Gaussian–Lorentz function. The dotted line represents the experimental peak, whereas the solid lines reflect the fitting data. Based on the interaction of NaF with blend electrolyte there are two possible interrelationships with CH$_2$ and CH stretching. Figure 3c shows the FTIR deconvolution for different NaF compositions. Absorbance peaks at 1427 cm^{-1} denote the anion vibration mode of C–H stretching, which proved the IR active in FTIR study. Figure 3d depicts the fundamental modes proved that peak at 2924 cm^{-1} was corresponding to CH$_2$ asymmetric stretching for NaF. As a result, the F^- band became extremely important in the study of ion dissociation in the polymer electrolyte system [29, 30]. The percentage of free ions/conduct ions of salt within the polymer host in C–H band region can be measured

Fig. 1 a Prepared solid polymer electrolyte and the flexibility. **b** Possible chemical interaction within the polymer matrix
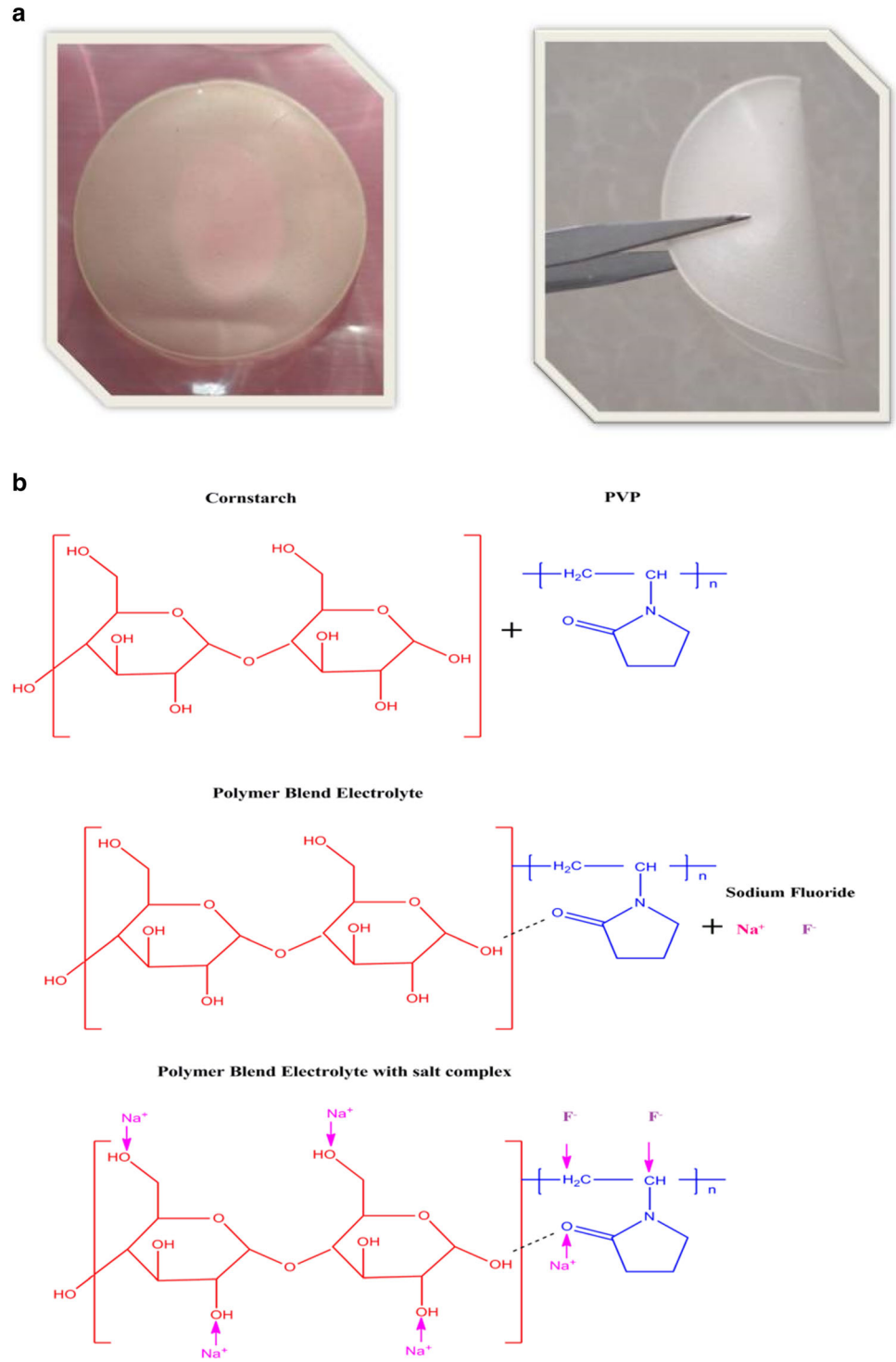

using the deconvolution technique using the following equation:

$$\text{Percentage of free ion } (\%) = (A_f / (A_f + A_c)) \times 100. \quad (1)$$

From the deconvoluted FTIR peaks, A_f is the total area of the free ion region and A_c is the total area of the contact ion region. As a result of the obvious ions interaction in CPF5, CPF10, CPF15, and CPF20, the region between 1480 and 1400 cm^{-1} was chosen for the percentage of free and contact ion calculation, the

Table 1 The quantity of chemicals in gms for the preparation of PBE

Cornstarch:PVP:NaF Composition in wt%	Cornstarch:PVP:NaF Composition in grams
80:20:5	0.8421:0.1443:0.0136
80:20:10	0.8307:0.1424:0.0269
80:20:15	0.8197:0.1405:0.0398
80:20:20	0.8090:0.1386:0.0524
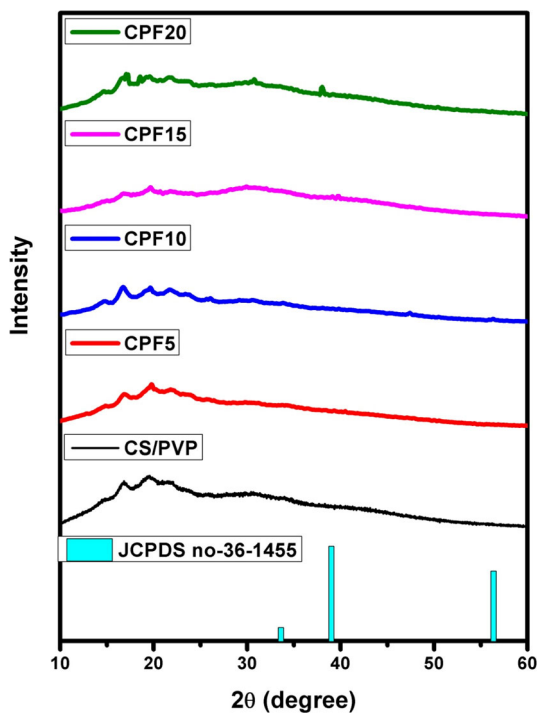
Fig. 2 X-ray diffraction pattern of CS/PVP, CPF5, CPF10, CPF15, and CPF20

calculated values are given in Table 3. The percentage of free ions in NaF-added polymer electrolyte is enhanced up to CPF15 due to increased ion dissociation [31, 32].

The system with CPF15 achieves the highest proportion of free ions. The percentage of free ions in electrolytes decreases beyond the indicated value CPF15 due to ion association. Hence, the peak of NaF at 1450 cm^{-1} and 1463 cm^{-1} is thought to be attributable to the free ion. Thus, the peak of NaF at 1425 cm^{-1} and 1450 cm^{-1} was assigned to the free anion and the peak at 1463 cm^{-1} is attributed to the contact ions [33, 34]. Higher conducting electrolyte attains highest value of 55.5% of free ion and lowest value of 44.5% of contact ion than the other concentration electrolytes. The presence of free and contact ions in the prepared electrolyte system is shown in Fig. 3c and d.

### 3.3 AC impedance spectroscopy

3.3.1 Cole–Cole plot

An impedance plot (Z'' vs. Z') is also known as the Nyquist plot, in which Z' describes the resistance area and Z'' values describe the capacitance area [35]. The conductivity of the prepared electrolytes are calculated based on the equation below:

$$\sigma = l/R_b A_e, \tag{2}$$

where l is the thickness of electrolyte, R_b is bulk resistance, and A_e is the electrode–electrolyte contact area. A screw gauge is used to measure the thickness of all solid polymer electrolytes [36]. Figure 4a shows the Cole–Cole plot observed from AC Impedance measurements of the CS/PVP, CPF5, CPF10, CPF15, and CPF20 electrolyte. Cole–Cole plot for the prepared samples shows a low-frequency spike with the high-frequency semicircle. The low-frequency spike is based on the polarization effect in the electrolyte–electrode conduct area. The semicircle is formed in the high-frequency region owing to the bulk resistance effect [37].

The equivalent circuit for the electrolytes is characterized by Z view fitting software and the calculated conductivity values of CS/PVP, CPF5, CPF10, CPF15, and CPF20 are listed in Table 4. Two sets of Parallel combination of resistance (R) and capacitance phase element (QPE) are used to fit the high-frequency semicircle region, which is based on supplementary interaction of salt and polymer chain and the spike is fitted by capacitance phase element (QPE) [12, 22, 29]. In all the prepared electrolytes, 15 wt% sodium fluoride-doped polymer sample shows maximum conductivity 4.6629×10^{-4} S cm^{-1} at room temperature (303 K).

Figure 4b shows the cole–cole CPF15 polymer sample which is heated to different temperatures. By way of the temperature increases, the bulk resistance reduces and leads to the improved conductivity of the sample [38].
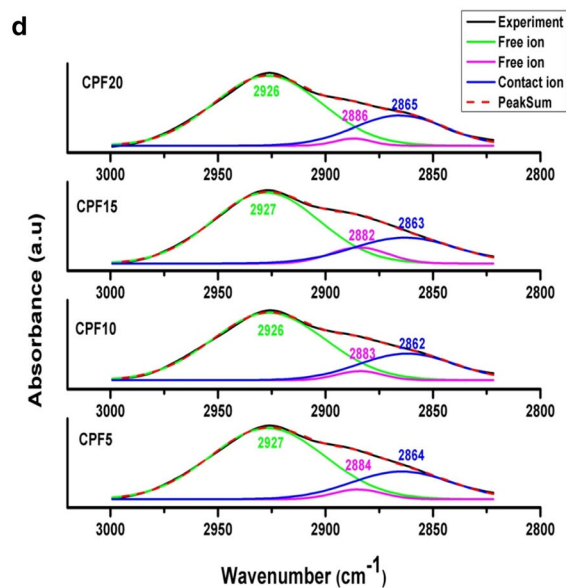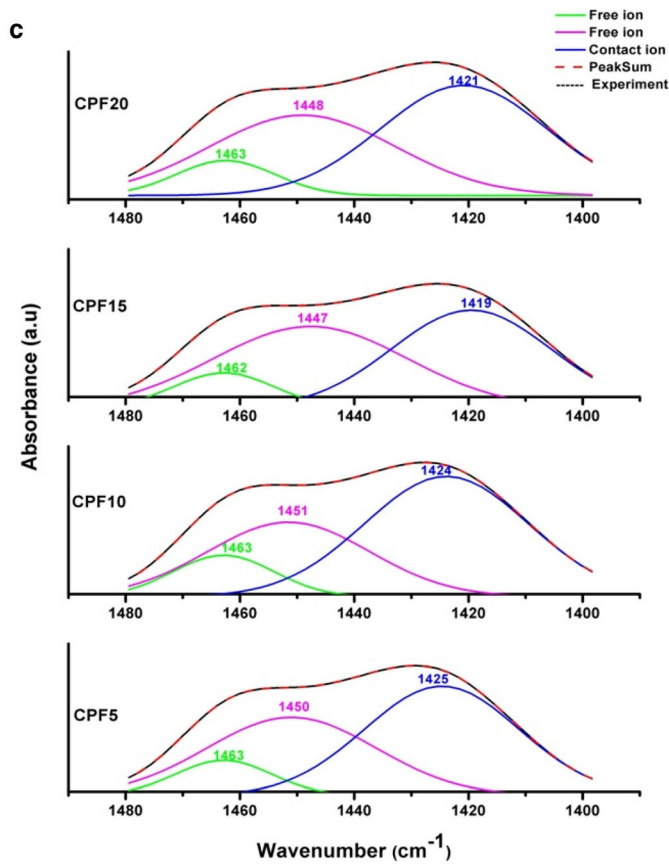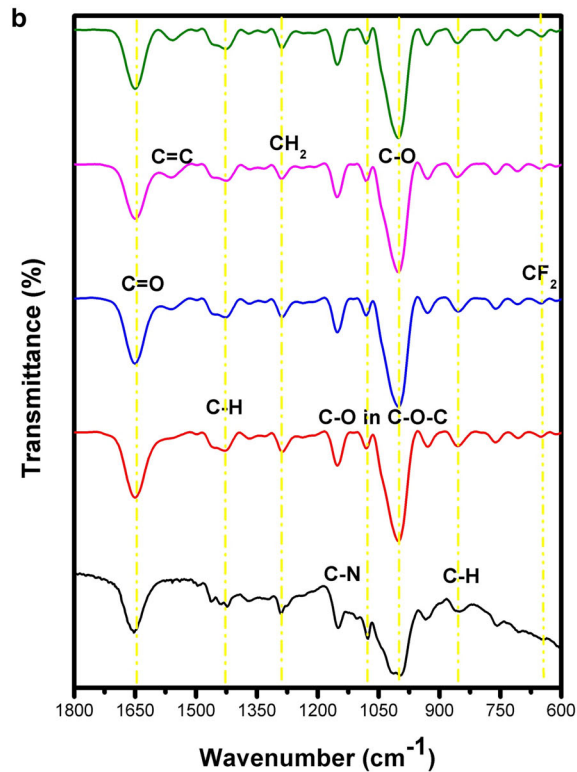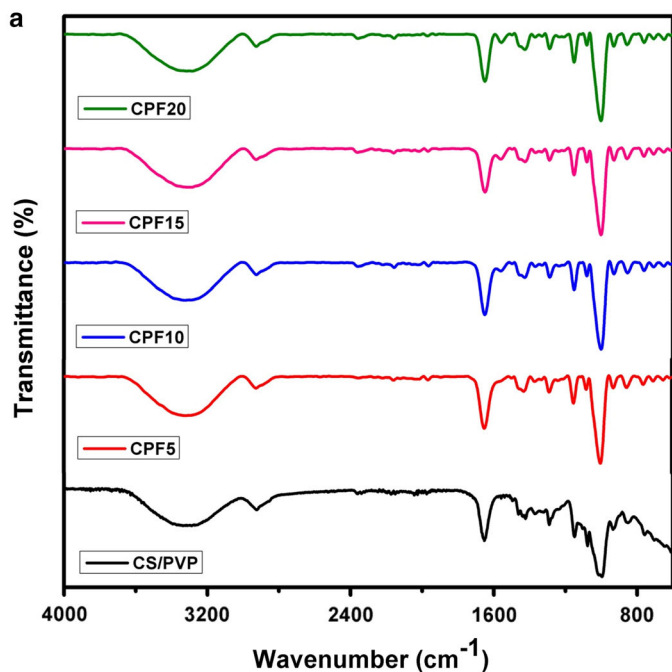
◀**Fig. 3 a** Fourier Transform Infrared analysis of CS/PVP and different wt% of sodium salt-doped system in 4000 cm^{-1} to 600 cm^{-1} range. **b** Fourier Transform Infrared analysis of CS/PVP and different wt% of sodium salt-doped system in 1800 cm^{-1} to 600 cm^{-1} range. **c** Deconvolution of the FTIR spectra at a wave number lies in the range of 1480–1400 cm^{-1}. **d** Deconvolution of the FTIR spectra at a wave number lies in the range of 3000–2800 cm^{-1}

Table 2 FTIR functional group analysis

Assignment	Wave number (cm^{-1})
O–H stretching	3323
CH$_2$ asymmetric stretching	2924
C=O Stretching	1655
C–H stretching	1427
CH$_2$ wagging	1422
C–N stretching	1288
C–O stretching	1147
C–O in C–O–C	995
C–C stretching	932
C–H asymmetric stretching	854
CF$_2$ bending	651

Table 3 FTIR deconvolution free ions and contact ions percentage

Sample	Free ion %	Contact ion %
CPF5	49.6	50.4
CPF10	45.2	54.8
CPF15	55.5	44.5
CPF20	50.1	49.9

3.3.2 Conduction spectra

Figure 5 represents the distinction of electrical conductivity with the function of frequency for the prepared electrolyte system. The conductivity behavioural aspect of CS/PVP, CPF5, CPF10, CPF15, and CPF20 has two distinct areas which are the high-frequency dispersion region by bulk relaxation and low-frequency independent plateau region [11]. Electrolyte CPF15 has a plateau region and logarithmic conductivity value slightly rises in the high-frequency region. In the low-frequency region, the DC conductivity can be determined by extending the plateau region on the (log σ) y-axis [18, 39].

The ionic conductivity from operating frequency for the prepared electrolyte and salt mixing electrolytes at 303 K temperature is discussed using Jonscher's general power law as follows:

$$\sigma(\omega) = \sigma_{\mathrm{o}} + A\omega^n, \tag{3}$$

where σ_{o} is the limiting zero frequency conductivity, A is the pre-exponential constant, and ω is the angular frequency [40]. However, the addition of different wt% of the salt leads to an increase in σ_{ac} value. CPF15 electrolyte attains a high conducting value of 4.6629×10^{-4} S cm^{-1} owing to the increase in the number of ions in the sample. Further, with the increase in salt concentration, conductivity value decreases [3].

3.3.3 Temperature-dependent conductivity

Figure 6 depicts the Arrhenius plot for different polymer blend electrolytes. The activation energy (E_{a}) is calculated by using the following expression:

$$\sigma = \sigma_{\mathrm{o}}\exp(-E_{\mathrm{a}}/k_{\mathrm{b}}T), \tag{4}$$

where σ_{o} is the pre-exponential factor, k_{b} is the Boltzmann constant, and T is the temperature. Activation energy is the energy required by ions to overcome the barrier to move freely. The movement of ions in this system follows the ion hopping mechanism. The conductivity increases as the temperature increases, some of the ions in the electrolyte acquire energy become free electrons and promote conduction [41, 42]. Calculated activation energy is 0.18 eV for higher conducting sample which is lower than the others [43]. Determined activation energy is given in Table 5.

3.3.4 Dielectric studies

Dielectric constant (ε') and dielectric loss (ε'') are detected over the frequency range 42 Hz to 1 MHz at room temperature. Figures 7 and 8 show the variation of ε' and ε'' with a function of frequency for CS/PVP blend with different wt% of sodium fluoride salt [44]. The real and imaginary parts of the complex permittivity have been premeditated by a relation [26].

$$\varepsilon^*(\omega) = \varepsilon'(\omega) - \mathrm{i}\,\varepsilon''(\omega) \tag{5}$$

The complex dielectric constant ε', and dielectric loss, ε'' are calculated as follows:
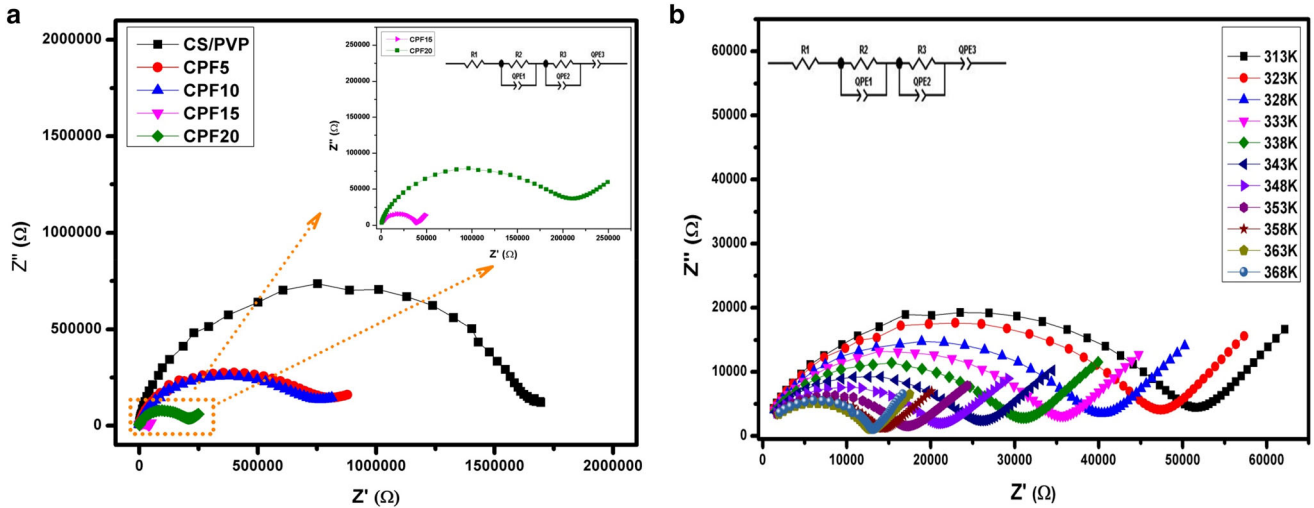
Fig. 4 **a** Cole–cole plot of CS/PVP blend and various wt% of sodium fluoride-added electrolytes. **b** Higher conducting sample CPF15 at different temperatures

Table 4 Calculated conductivity value using bulk resistance R_b value

Sample	Conductivity σ_{ac} (S cm^{-1})
CS/PVP	5.3405×10^{-9}
CPF5	3.3413×10^{-5}
CPF10	4.0955×10^{-5}
CPF15	4.6629×10^{-4}
CPF20	9.7919×10^{-5}

Fig. 6 Plot of 1000/T versus logarithmic conductivity value

Table 5 Activation energy for the prepared electrolytes

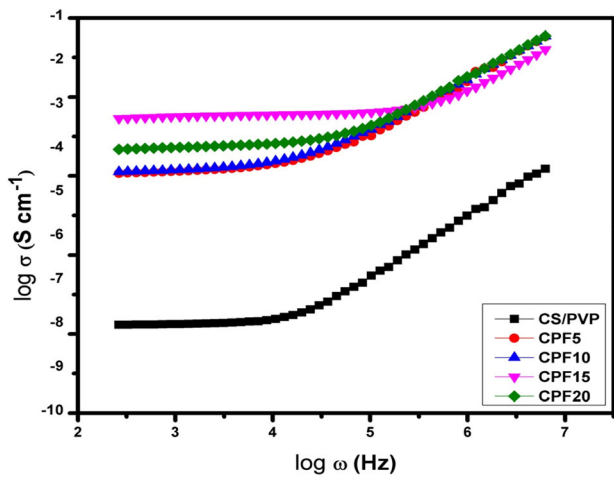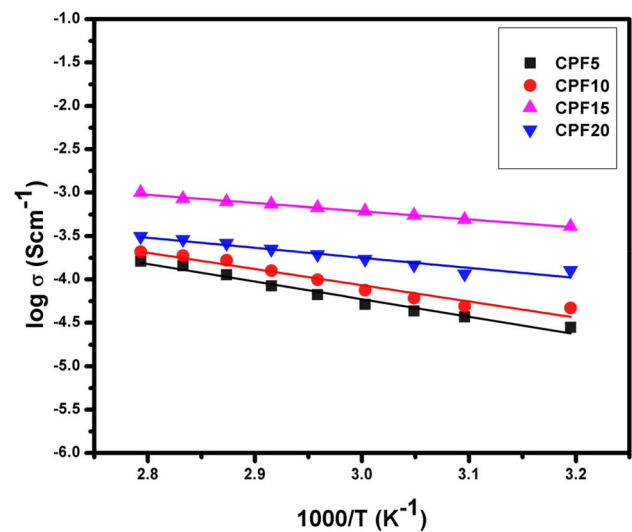| Sample	Activation energy E_a
CPF5	0.3858
CPF10	0.3558
CPF15	0.1775
CPF20	0.2204

Fig. 5 logarithmic angular frequencies (ω) versus conductance (σ) for all the prepared samples at ambient temperature

$$\varepsilon'(\omega) = Z''/\omega C_0\left(Z'^2 + Z''^2\right) \tag{6}$$

$$\varepsilon''(\omega) = Z'/\omega C_0\left(Z'^2 + Z''^2\right) \tag{7}$$

From Figs. 7a and 8a, the frequency dependence of $\varepsilon'(\omega)$ and $\varepsilon''(\omega)$ at room temperature can be explained about the space charge polarization effect at the electrode–electrolyte interface. The dielectric
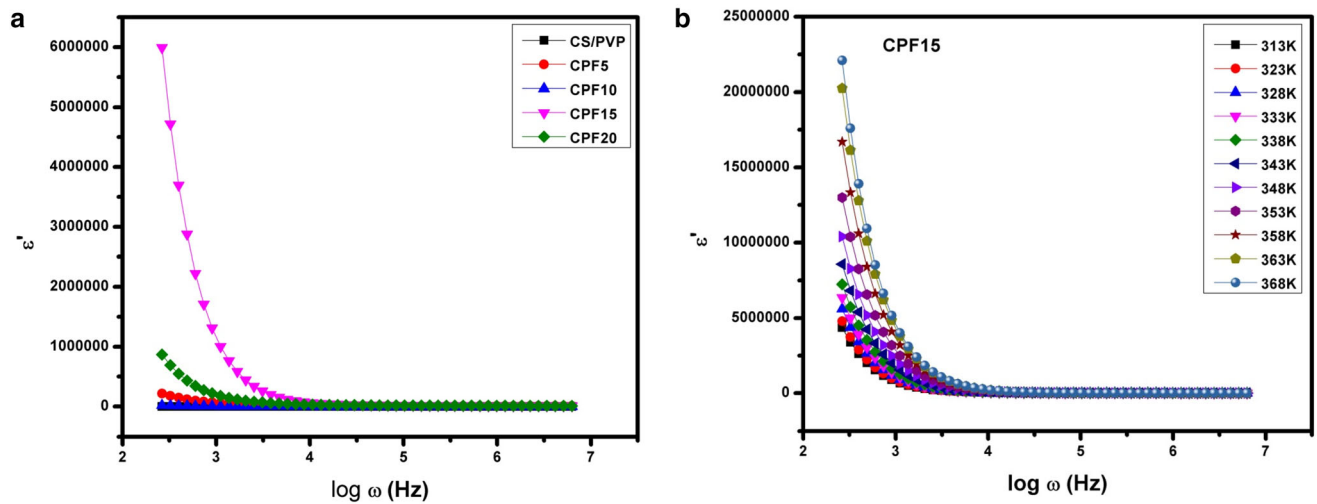
Fig. 7 a Dielectric constant ε' versus log ω for CS/PVP, CPF5, CPF10, CPF15, and CPF20. **b** Dielectric constant ε' versus log ω for higher conducting sample CPF15 with different temperatures

Fig. 8 a Dielectric loss ε'' versus log ω for CS/PVP, CPF5, CPF10, CPF15, and CPF20. **b** Dielectric loss ε'' versus log ω for higher conducting sample CPF15 with different temperatures
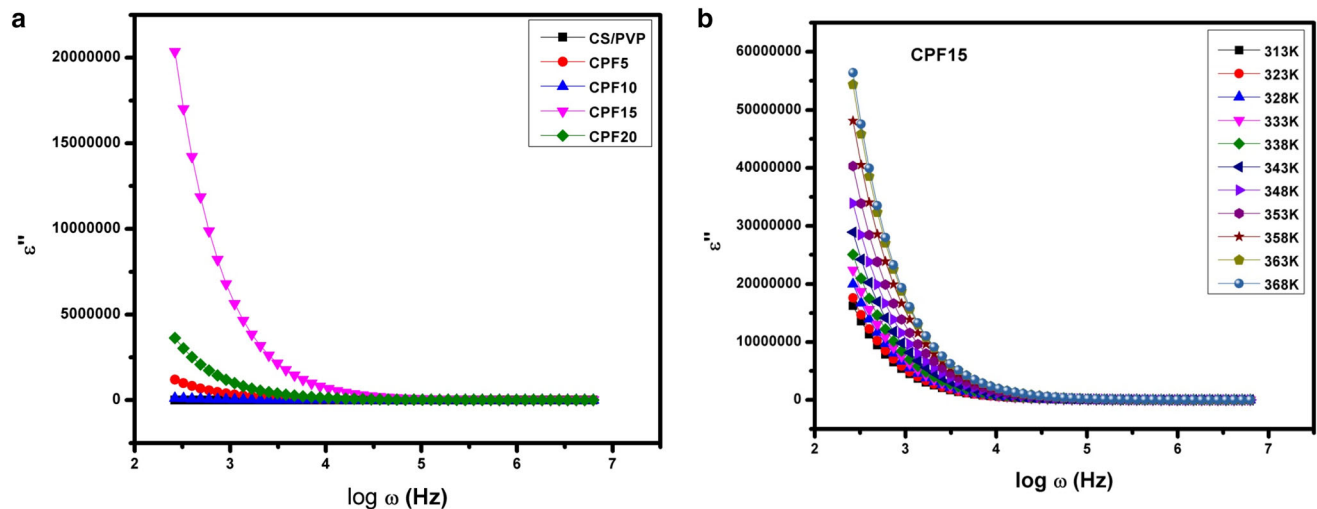
permittivity value of CPF15 is higher than CS/PVP electrolyte at low frequencies. The periodic reversal of the field occurs when the frequency increases, dielectric permittivity (ε' (ω), ε'' (ω)) is initiated to reduce and become zero for all samples. It represents there is no conceivable orientation for the charge carriers in the field direction as well as there is less diffusion of charge carriers towards the field direction [44].

Figures 7b and 8b denote the dielectric studies of higher conducting sample (CPF15) with the increase of temperature, dielectric permittivity and loss both are increased. The reason is that the free-moving ions

get more energy and this creates the ions to line up with the externally applied field by increasing the temperature. Hence, at low temperatures, mobile ions fail to line up at the externally applied field owing to low energy content [45, 46].

3.3.5 Modulus spectra

AC impedance spectrum provides electrical behaviour in the low-frequency range. Modulus studies give more information about dielectric behaviour. The equations for real electrical modulus M' and imaginary modulus M'' can be expressed as follows:

$$M' = \varepsilon'/\left(\varepsilon'^2 + \varepsilon''^2\right) \qquad (8)$$

$$M'' = \varepsilon''/\left(\varepsilon'^2 + \varepsilon''^2\right) \qquad (9)$$

Figures 9 and 10 show the real (M') and imaginary (M'') part of the electric modulus, respectively [47, 48]. At the low-frequency region, M' and M'' decrease due to the electrode polarization process and a long tail is observed in the plot and it confirms a large capacitance related with electrodes [49].

This confirms the non-Debye behaviour in the samples. From Fig. 9a, the value of M' rises with increasing frequency and touches the maximum at higher frequency lacking relaxation peaks, which is owing to the supply of relaxation processes over a range of frequencies [50]. Figures 9b and 10b plots show the variation of M' and M'' with temperature for the higher conducting sample CPF15. As temperature rises, the value of the electric modulus moves towards a higher frequency [41].

3.3.6 Argond plot

The bulk dielectric effect of the higher conducting sample is interpreted from complex modulus spectra. Figure 11 represents the argond plot of sample CPF15 observed at different temperatures. The spectrum explained the occurrence of the imperfect semicircle. Primarily, dielectric data can be changed into modulus data and complex modulus (M^*) which are stated as [3, 11, 51, 52]

$$M^* = M'(\omega) + jM''(\omega) \qquad (10)$$

$$M^* = j/C_0 Z^* \qquad (11)$$

From Fig. 11 the curves reveal clearly incomplete semicircles, indicating non-Debye behaviour. The radius of the semicircle arcs reduces as the temperature increases and it is confirms the improvement in conductivity. When the radius of the semicircle arc is reduced, the ions' relaxation time in polymer electrolytes is also shortened [3].

3.3.7 Tangent studies

Figure 12 illustrates tan δ with the variation of frequency for CS/PVP, CPF5, CPF10, CPF15, and CPF20 at 303 K temperature. The dielectric loss tangent can be defined as

$$\tan\delta = \varepsilon''/\varepsilon' \qquad (12)$$

The wide dispersion peak detected at low frequencies could be accredited to the interfacial polarization mechanism. The sharp dispersion detected at the highest frequencies could be credited to the dipolar relaxation [12]. For the Salt mixed system, the height of the hump is enlarged and get rid of the higher frequency side signifying the increase of movement of charge carriers [11, 38]. The alignment of polar groups is estimated to be associated for the dielectric relaxation phenomenon. The dielectric relaxation time can be calculated with the equation $\omega\tau = 1$. ω represents the peak frequency and τ
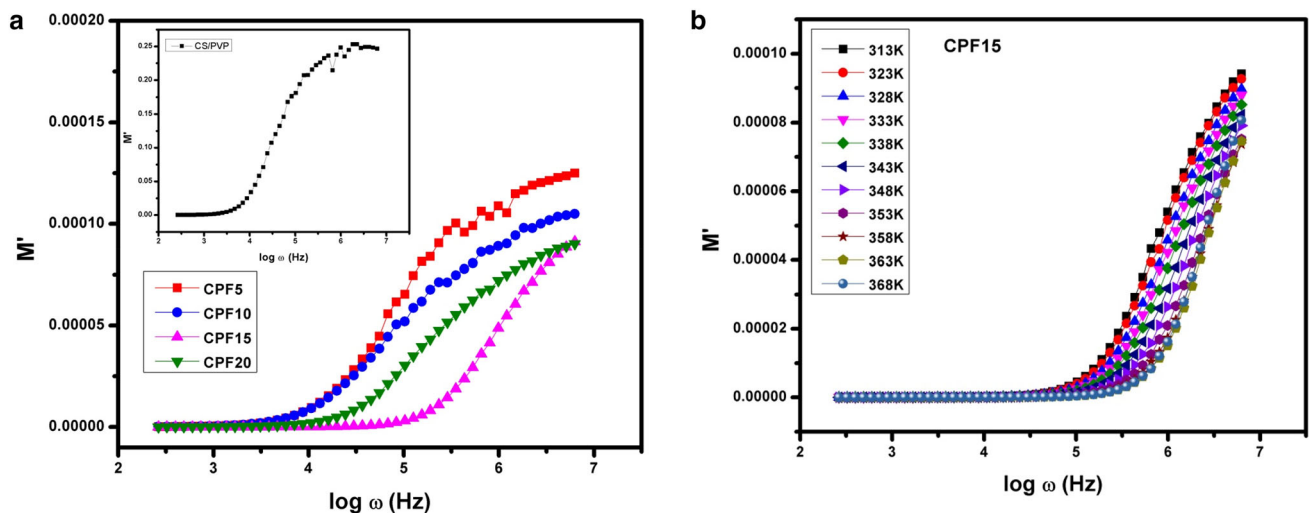

Fig. 9 **a** Real part of electric modulus for salt dopant system then the inserted plot represents M' for blend system. **b** Real part of modulus (M') with different temperatures for CPF15

a

b
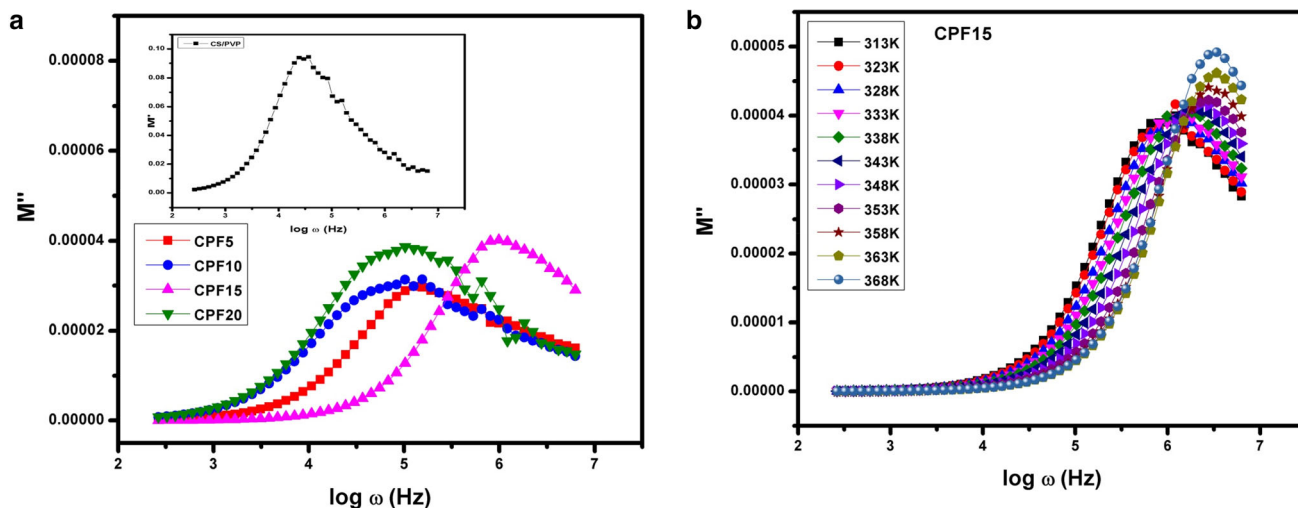

Fig. 10 a Imaginary part of electric modulus (M'') of CS/PVP and salt dopant system. b Imaginary part of modulus (M'') with different temperatures for CPF15
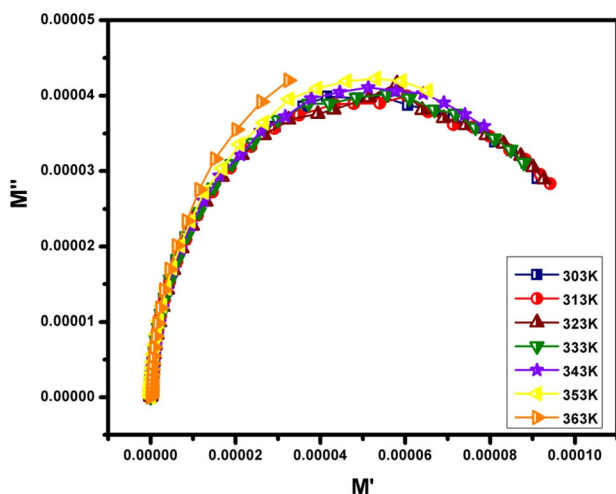

Fig. 11 Argond plot for higher conducting sample at various temperatures

Fig. 12 Tangent Analysis (tan δ) for CS/PVP, CPF5, CPF10, CPF15, and CPF20

represents relaxation time of the electrolyte. According to the determined relaxation time, once the salt concentration increases, the relaxation time decreases up to the CPNC10 sample. These higher conducting samples achieve the lowest relaxation time. The relaxation time value for CPNC12 was enhanced.

$$\phi(t) = \exp(-t/\tau)^{\beta}, \qquad (13)$$

where τ and β are tangent relaxation time and the Kohlrausch exponent, respectively. The minimum value of τ indicates the more electrical relaxation process [43]. Using the formula $\beta = 1.14/\text{FWHM}$ exponent value of all the prepared compositions is
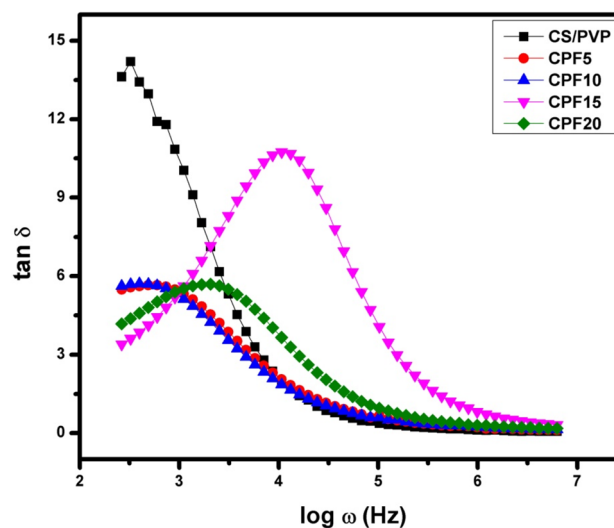
calculated. The β values are listed in Table 6 indicating the non-Debye nature of the electrolytes [53].

3.3.8 Transference number studies (TNS)

The ionic and electronic transport for conductivity can be determined by Wagner's DC polarization technique. A dc potential of 2 V is applied in between graphite-coated silver electrodes which act as blocking electronic transport and silver electrode. Current is taken as a function of time until the constant state has appeared. The initial current is decreased with the increase of time [25, 32] which is shown in Fig. 13.

Table 6 Value of relaxation time and Kohlrausch exponent parameter

Sample	Relaxation time τ (s)	FWHM	β
CPF5	2.5457×10^{-3}	2.5093	0.4543
CPF10	2.0089×10^{-3}	2.4381	0.4675
CPF15	9.3562×10^{-5}	1.7885	0.6374
CPF20	4.8489×10^{-4}	2.5367	0.4494

$$t_+ = I_i - I_f / I_i \tag{14}$$

$$t_- = I_f / I_i, \tag{15}$$

where t_+ represents transport number of ions; t_- represents transport number of electron; I_f represents final current; I_i represents initial current [1]

The calculated transference numbers of the prepared electrolytes are listed in Table 7. The ionic transport number is 0.98 for higher conducting sample CPF15. This value is closer to unity. From this, it is confirmed that ionic transport is higher than electronic transport for prepared electrolyte [2].

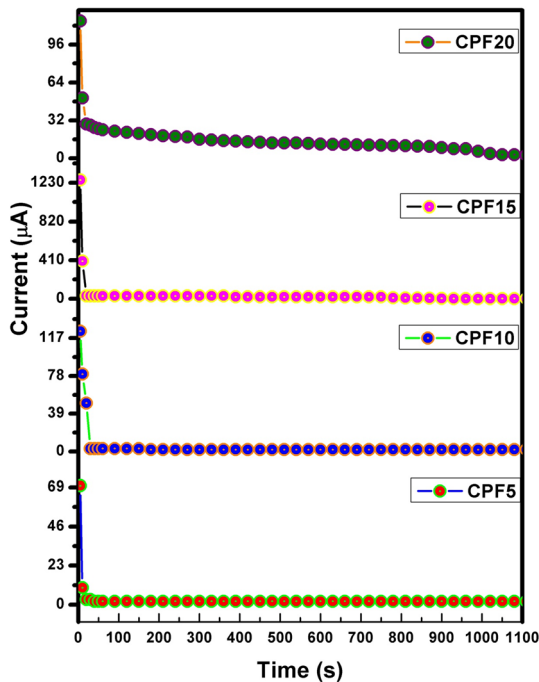$$n = (N\rho \times \text{ molar ratio of salt})/\text{molar weight of the salt}$$

where N = Avogadro's number (6.023×10^{23} particles per mole), ρ = Density of the salt (NaF = 2.56 g cm^{-3}).

Transference number (t_{ele} and t_{ion}) and Conductivity (σ) are used to calculate the following parameters:

$$D = D_+ + D- = KT\sigma/ne^2 \tag{16}$$

$$t_{ion} = D_+ / D_+ + D_- \tag{17}$$

$$t_{ele} = D_- / D_+ + D_- \tag{18}$$

$$\mu = \mu_+ + \mu_- = \sigma/ne \tag{19}$$

$$t_{ion} = \mu_+ / \mu_+ + \mu_- \tag{20}$$

$$t_{ele} = \mu_- / \mu_+ + \mu_-, \tag{21}$$

where D diffusion coefficient (cm^2 s^{-1}); K Boltzman constant (1.3806×10^{-23} m^2 kg s^{-2} K^{-1}); σ Conductivity of the sample (S cm^{-1}); e Charge of the electron (1.602×10^{-19} C); μ Mobility (cm^2 Vs^{-1}) [11]

Up to 15 wt% of NaF-added system, the conductivity increases and a similar pattern is seen in the diffusion coefficient and ionic mobility of cations and anions, which is displayed in Table 7. Along these lines, the transference number uncover the end that higher values of D_+ and μ_+ are responsible for the higher ion conductivity [11]. For CPF20, there is an increase of charge carries and a decrease of mobility which is due to collision of charge carrier in the lattice. So, the Conductivity of CPF20 sample is decreased.

3.3.9 CV plot

The stability and electrochemical behaviour of the electrolyte can be discussed using cyclic voltammetry [51]. Cyclic voltammetry is executed in the potential window (− 0.06 to 0.06 V) at various scan rates. Figure 14 represents CV curves of CPF15 electrolyte [54]. The intrinsic Faradaic reaction current of 50 mV s^{-1} was much higher than that of the low scan rate. All Scan rates of 5 mV s^{-1}, 10 mV s^{-1}, 25 mV s^{-1}, and 50 mV s^{-1} in CV curves show two clear symmetric peaks showing up in the negative and positive scans, suggesting the amazing reversibility of the Faradaic responses [55].

The closed loops of CV curve represent good electrochemical performance possibility. CV curves of the CPF15 for various cycles show symmetry shape

Fig. 13 Transference number analysis for different wt% of NaF-added electrolytes

Table 7 Transport parameters of different wt% of NaF-added CS/PVP blend systems

Weight of salt in %	No. of charge carriers (n) in cm^{-3}	Transference number		Diffusion coefficient in cm^2 s^{-1}			Mobility (μ) in cm^2 Vs^{-1}		
		T_{ion}	T_{ele}	D	D_+	D_-	μ	μ_+	μ_-
5	$5.16034 \times 10^{+20}$	0.9714	0.0285	1.06×10^{-8}	1.03×10^{-8}	3.02×10^{-10}	4.05×10^{-7}	3.93×10^{-7}	1.16×10^{-8}
10	$1.03207 \times 10^{+21}$	0.9834	0.0161	6.48×10^{-9}	6.38×10^{-9}	1.05×10^{-10}	2.48×10^{-7}	2.44×10^{-7}	4.00×10^{-9}
15	$1.5481 \times 10^{+21}$	0.9841	0.0158	4.92×10^{-8}	4.84×10^{-8}	7.81×10^{-10}	1.88×10^{-6}	1.85×10^{-6}	2.99×10^{-8}
20	$2.06414 \times 10^{+21}$	0.9827	0.0172	7.75×10^{-9}	7.62×10^{-9}	1.34×10^{-9}	2.96×10^{-7}	2.91×10^{-7}	5.11×10^{-7}
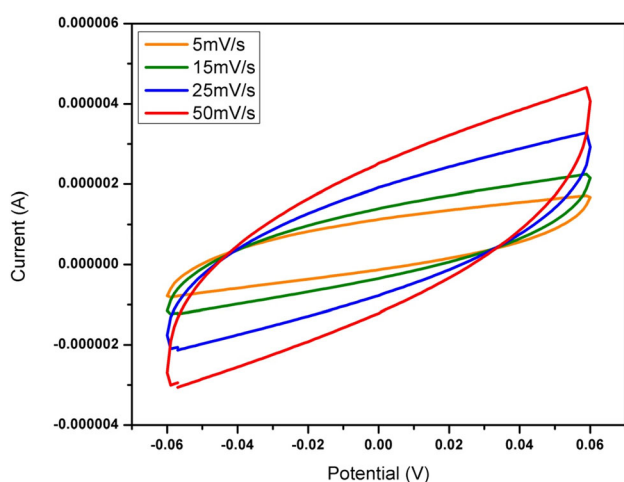
Fig. 14 Cyclic voltammetry behaviours of the CPF15 samples

of oxidation and reduction peaks, which confirms the better electrochemical action [56–58].

4 Conclusion

CS/PVP blends with different concentrations of sodium fluoride polymer samples are prepared by the solution casting process. The XRD patterns confirm the CS/PVP blend polymer samples. The addition of salt with the polymer blend improves the decreased intensity peak. FTIR studied clearly explained the presence of blend polymers by the functional groups and the addition of salt developed shifts in wavenumber. The highest conductivity obtained for CPF15 sample is 4.6629×10^{-4} S cm^{-1}. Dielectric studies explained that with the increase of temperature, dielectric permittivity constant and loss both are increased for all samples. The effects of electrode polarization were observed from modulus studies. Argond plot explained the relaxation process. The tangent loss peak used to calculate the

relaxation time (τ), FWHM, β for CPF15 sample is 9.3562×10^{-5} s, 1.7885, and 0.6374, respectively. The diffusion coefficient and mobility of cations are higher than anions and maximum for CPF15. The Faradic behaviour of this higher conducting sample has been observed from the Cyclic Voltammetry study. From this, it is suggested that this eco-friendly, cost-effective biopolymer electrolyte could be used for energy storage device applications.

Author contributions

All authors contributed to the study conception and design. Material preparation, data collection, and analyses were performed by MN. The first draft of the manuscript was written by Dr. DV and all authors commented on previous versions of the manuscript. All authors read and approved the final manuscript.

Data availability

The datasets generated during and/or analysed during the current study are available from the corresponding author on reasonable request.

Declarations

References

1. R. Chitra, P. Sathya, S. Selvasekarapandian, S. Meyvel, Polym. Bull. **77**, 1555 (2020)

2. S. Shanmuga Priya, M. Karthika, S. Selvasekarapandian, R. Manjuladevi, S. Monisha, Ionics **24**, 3861 (2018)

3. K. Sundaramahalingam, D. Vanitha, N. Nallamuthu, A. Manikandan, M. Muthuvinayagam, Phys. B **553**, 120 (2019)

4. G. Boopathi, S. Pugalendhi, S. Selvasekarapandian, M. Premalatha, S. Monisha, G. Aristatil, Ionics **23**, 2781 (2017)

5. A. Arya, A.L. Sharma, J. Mater. Sci. **29**, 17903 (2018)

6. D. Xie, M. Zhang, Y. Wu, L. Xiang, Y. Tang, Adv. Funct. Mater. **30**, 1 (2020)

7. T. Tiwari, J.K. Chauhan, M. Yadav, M. Kumar, N. Srivastava, Ionics **23**, 2809 (2017)

8. A. H. A. Syakirah binti Shahrudin, Solid State Phenom. **268**, 347 (2017)

9. Y.M. Yusof, M.F. Shukur, H.A. Illias, M.F.Z. Kadir, Phys. Scr. **89**, 035701 (2014)

10. S. Ramesh, R. Shanti, E. Morris, J. Mol. Liq. **166**, 40 (2012)

11. N. Nallamuthu, M. Manikandan, A. Anandha Jothi, D. Vanitha, S. Asath Bahadur, Phys. B **580**, 411940 (2020)

12. D. Vanitha, S.A. Bahadur, N. Nallamuthu, S. Athimoolam, A. Manikandan, J. Inorg. Organomet. Polym. Mater. **27**, 257 (2017)

13. S.K.S. Basha, G.S. Sundari, K.V. Kumar, M.C. Rao, J. Inorg. Organomet. Polym. Mater. **27**, 455 (2017)

14. B. Jinisha, K.M. Anilkumar, M. Manoj, P. Pradeep, J. Jayalekshmi, Electrochim. Acta **235**, 210 (2017)

15. K.K. Kumar, Y. Pavani, M. Ravi, S. Bhavani, A.K. Sharma, V.V.R.N. Rao, AIP Conf. Proc. **1391**, 641 (2011)

16. K.K. Kumar, M. Ravi, Y. Pavani, S. Bhavani, A.K. Sharma, V.V.R. Narasimha Rao, J. Membr. Sci. **454**, 200 (2014)

17. H.K. Koduru, L. Marino, F. Scarpelli, A.G. Petrov, Y.G. Marinov, G.B. Hadjichristov, M.T. Iliev, N. Scaramuzza, Curr. Appl. Phys. **17**, 1518 (2017)

18. M. Irfan, A. Manjunath, S.S. Mahesh, AIP. Conf. Proc. **2244**, 5 (2020)

19. P.B. Bhargav, V.M. Mohan, A.K. Sharma, V.V.R.N. Rao, Curr. Appl. Phys. **9**, 165 (2009)

20. K.K. Kumar, M. Ravi, Y. Pavani, S. Bhavani, A.K. Sharma, Physica B **406**, 1706 (2011)

21. M.A. Jothi, D. Vanitha, S.A. Bahadur, Int. J. Recent Technol. **887** (2019)

22. M.A. Jothi, D. Vanitha, S.A. Bahadur, N. Nallamuthu, J. Mater. Sci. **32**, 5427 (2021)

23. M. Ravi, K. Kiran Kumar, V. Madhu Mohan, V.V.R. Narasimha Rao, Polym. Test. **33**, 152 (2014)

24. A.P. Apisarov, A.E. Dedyukhin, A.A. Red, O.Y. Tkacheva, Y.P. Zaikov, Elektrokhimiya **46**, 672 (2010)

25. N. Adiera, H. Rosli, K.S. Loh, W.Y. Wong, R.M. Yunus, T.K. Lee, A. Ahmad, S.T. Chong, Int. J. Mol. Sci. **21**, 632 (2020)

26. P. Sangeetha, T.M. Selvakumari, S. Selvasekarapandian, S.R. Srikumar, R. Manjuladevi, M. Mahalakshmi, Ionics **26**, 233 (2020)

27. M.F. Shukur, R. Ithnin, M.F.Z. Kadir, Electrochim. Acta **136**, 204 (2014)

28. S. Kiruthika, M. Malathi, S. Selvasekarapandian, K. Tamilarasan, T. Maheshwari, Polym. Bull. **77**, 6299 (2020)

29. M.A. Jothi, D. Vanitha, S.A. Bahadur, N. Nallamuthu, Bull. Mater. Sci. **44**, 1 (2021)

30. A.S. Mohamed, M.F. Shukur, M.F.Z. Kadir, Y.M. Yusof, J. Polym. Res. **27**, 1–14 (2020)

31. P. Moni, J. Solid State Electrochem. **25**, 2371 (2021)

32. C.M. Cholant, M.P. Rodrigues, L.L. Peres, R.D.C. Balboni, L.U. Krüger, D.N. Placido, W.H. Flores, A. Gündel, A. Pawlicka, C.O. Avellaneda, J. Solid State Electrochem. **24**, 1867 (2020)

33. S.B. Aziz, E.M.A. Dannoun, M.H. Hamsan, H.O. Ghareeb, M.M. Nofal, W.O. Karim, A.S.F.M. Asnawi, J.M. Hadi, M.F.Z.A. Kadir, Polymers **13**, 930 (2021)

34. H. Uğuz, A. Goyal, T. Meenpal, I.W. Selesnick, R.G. Baraniuk, N.G. Kingsbury, A. Haiter Lenin, S. Mary Vasanthi, T. Jayasree, M. Adam, E.Y.K. Ng, S.L. Oh, M.L. Heng, Y. Hagiwara, J.H. Tan, J.W.K. Tong, U.R. Acharya, G. Cappiello, S. Das, E.B. Mazomenos, K. Maharatna, G. Koulaouzidis, J. Morgan, P.E. Puddu, M.A. Goda, P. Hajas, G.D. Clifford, C. Liu, B. Moody, D. Springer, I. Silva, Q. Li, R.G. Mark, D. Kristomo, R. Hidayat, I. Soesanti, A. Kusjani, I. Grzegorczyk, M. Solinski, M. Lepek, A. Perka, J. Rosinski, J. Rymko, K. Stepien, J. Gieraltowski, A. Ghaffari, M.R. Homaeinezhad, M. Khazraee, M.M. Daevaeiha, J. Xu, L.G. Durand, P. Pibarot, S.K. Randhawa, M. Singh, J. Robinson, K. Xi, R.V. Kumar, A.C. Ferrari, H. Au, M.-M. Titirici, A. Parra Puerto, A. Kucernak, S.D. S. Fitch, N. Garcia-Araez, J. Herzig, A. Bickel, A. Eitan, N. Intrator, J. Robinson, K. Xi, R.V. Kumar, A.C. Ferrari, H. Au, M.-M. Titirici, A. Parra Puerto, A. Kucernak, S.D.S. Fitch, N. Garcia-Araez, H. Search, C. Journals, A. Contact, M. Iopscience, I.P. Address, A.M. Rahman, T.A. Manuscript, I.O.P. Publishing, A. Manuscript, A. Manuscript, C.C. By-nc-nd, A. Manuscript, C. Liu, D. Springer, G.D. Clifford, D. verma Atul, Y.H. Lei Shao, Q. Gao, Xie, J. Fu, M. Xiang, E. Kay, A. Agarwal, M. Gjoreski, A. Gradisek, B. Budna, M. Gams, G. Poglajen, H. Li, Y. Ren, G. Zhang, R. Wang, J. Cui, W. Zhang, A. K. Dwivedi, S. A. Imtiaz, and E. Rodriguez-Villegas, J. Phys. Energy **2** (2020)

35. A. Baral, K.R.S. Preethi Meher, K.B.R. Varma, Bull. Mater. Sci. **34**, 53 (2011)

36. M.F. Shukur, M.F.Z. Kadir, Ionics. **21**, 111 (2015)

37. M.A. Jothi, D. Vanitha, S.A. Bahadur, N. Nallamuthu, Ionics **27**, 225 (2021)

38. K. Sundaramahalingam, M. Muthuvinayagam, N. Nallamuthu, D. Vanitha, M. Vahini, Polym. Bull. **76**, 5577 (2019)

39. M. Muthukrishnan, C. Shanthi, S. Selvasekarapandian, R. Manjuladevi, P. Perumal, P. Chrishtopher Selvin, Ionics **25**, 203 (2019)

40. V. Duraikkan, A.B. Sultan, N. Nallaperumal, A. Shunmuganarayanan, Ionics **24**, 139 (2018)

41. T. Sugumaran, D.S. Silvaraj, N.M. Saidi, N.K. Farhana, S. Ramesh, K. Ramesh, S. Ramesh, Ionics **25**, 763 (2019)

42. R. Punia, R.S. Kundu, M. Dult, S. Murugavel, N. Kishore, R. Punia, R.S. Kundu, M. Dult, S. Murugavel, N. Kishore, J. Appl. Phys. **112**, 083701 (2012)

43. Z. Imran, M.A. Rafiq, M. Ahmad, K. Rasool, S.S. Batool, M.M. Hasan, AIP Adv. **3**, 1 (2013)

44. R. Chitra, P. Sathya, S. Selvasekarapandian, S. Meyvel, Mater. Res. Express **7**, 015309 (2019)

45. N.N. Mobarak, F.N. Jumaah, M.A. Ghani, M.P. Abdullah, A. Ahmad, Electrochim. Acta **175**, 224 (2015)

46. V. Siva, A. Shameem, A. Murugan, M.A. Jothi, M. Suresh, S. Athimoolam, J. Mater. Sci. **31**, 17921–17930 (2020)

47. P. Barai, K. Higa, V. Srinivasan, Phys. Chem. Chem. Phys. **19**, 20493 (2017)

48. M.S.A. Rani, N.A. Dzulkurnain, A. Ahmad, N.S. Mohamed, Int. J. Polym. Anal. Charact. **20**, 250 (2015)

49. A.K. Arof, N.E.A. Shuhaimi, N.A. Alias, M.Z. Kufian, S.R. Majid, J. Solid State Electrochem. **14**, 2145 (2010)

50. Y. Moualhi, M.M. Nofal, R. M'nassri, H. Rahmouni, A. Selmi, M. Gassoumi, K. Khirouni, A. Cheikrouhou, Ceram. Int. **46**, 1601 (2020)

51. J.L. Izquierdo, G. Bolaños, V.H. Zapata, O. Morán, Curr. Appl. Phys. **14**, 1492 (2014)

52. M. Ravi, S. Bhavani, K. Kiran Kumar, V.V.R. Narasimaha Rao, Solid State Sci. **19**, 85 (2013)

53. G. Hirankumar, S. Selvasekarapandian, M.S. Bhuvaneswari, R. Baskaran, M.Vijayakumar, Solid State Electrochem. **10**, 193 (2006)

54. N. Farah, H.M. Ng, Arshid Numan, Chiam-Wen Liew N.A.A. Latip, K. Ramesh, S. Ramesh, Mater. Sci. Eng. B **251**, 114468 (2019)

55. H.J. Woo, S.R. Majid, A.K. Arof, Mater. Chem. Phys. **134**, 755 (2012)

56. S. Rudhziah, N.A.C. Apandi, R.H.Y. Subban, N.S. Mohamed, Sci. Lett. **12**, 45 (2018)

57. S.B. Aziz, M.H. Hamsan, M.M. Nofal, W.O. Karim, I. Brevik, M.A. Brza, R.T. Abdulwahid, S. Al-Zangana, M.F.Z. Kadir, Polymers **12**, 1885 (2020)

58. J.G. Reynolds, J.D. Belsher, J. Chem. Eng. Data **62**, 1743 (2017)